Bulk-assembly of monodisperse coacervates and giant unilamellar vesicles with programmable hierarchical complexity

Qingchuan Li[1, 2, #, *], Qingchun Song[2, #], Jing Wei[1], Yang Cao[2], Xinyu Cui[3], Dairong Chen[1, *], Ho Cheung Shum[2, *]

[1]School of Chemistry & Chemical Engineering, National Engineering Research Center for Colloidal Materials, Shandong University, Jinan 250100, P. R. China.
[2]Department of Mechanical Engineering, The University of Hong Kong, Pokfulam Road, Hong Kong, China
[3]Department of Public Health, Mudanjiang Medical University, Mudanjiang 157000, P. R. China

*Correspondence to: ashum@hku.hk; cdr@sdu.edu.cn; lqc3038@hku.hk
[#]These authors contributed equally to this work

Abstract.
Compartmentalization is an essential step for the emergence of protocellular life on the early earth and the endeavor to bottom-up construct synthetic cells in the lab. Among manifold natural strategies for compartmentalization, assembly of lipid vesicles or coacervate droplets with resemblance to cell envelope or cytoplasm have emerged as two dominant paradigms. However, the spontaneous assembly of lipid vesicles or coacervates generally results in polydisperse microcompartments and lacks the ability to efficiently integrate functional building blocks towards defined complexity, which give rise to the difficulty to achieve the order and complexity towards the scope of that of life via spontaneous assembly. Herein, we show that the interplay of coacervates and colloidal particles provides a bulk-assembly approach to form monodisperse coacervates and giant unilamellar vesicles (GUVs) with programmable hierarchical complexity. The hierarchical complexity of the synthetic cell microcompartments can be delicately engineered from the control of the spatial or temporal organization of components in entity unit to manifold forms of interconnected synthetic cell consortia, achieving a compartment hierarchy analogous to the organelle-cell-tissue structure. The increase in complexity gives rise to emergent properties, for instance, collective morphology evolution of coacervate assemblages, gated permeability of GUVs without sophisticated protein machinery, and remarkable structural and functional stability of GUVs at extreme conditions. This work paves an unprecedented step to form monodisperse, hierarchical coacervates and GUVs via bulk-assembly, which provides a prebiotically plausible approach for the proper integration of inanimate matter towards the order and complexity of life and monodisperse, hierarchical microdroplets for follow-up scientific and technological applications.

Introduction

Bottom-up synthetic biology is an emerging field of science aimed at constructing minimal living systems from the inanimate[1,2]. This endeavor could promisingly shed light on the origin and functional principle of cellular life and invigorate applications such as bioreactors and advanced delivery systems[3-6]. For synthetic cell construction, a primary step is to fabricate a compartment for the spatially and temporally controlled integration of basic functional components[7]. During the last past years, various synthetic cell architectures, such as fatty acid vesicles[8], liposomes[9,10], polymersomes[11], proteinosomes[12], emulsions[13,14], coacervate droplets[15-17] and some hybrid systems[18,19], have been developed as compartments for the spatial localization and isolation of molecules and their reactions. Among them, lipid vesicles and coacervate droplets have been extensively utilized as scaffolds to engineer synthetic cells due to their structural resemblance to cell envelope or cytoplasm, as well as prebiotic relevance to life emergence.

Microfluidic methods have provided great promise in recent years for the generation of lipid vesicles or coacervates with defined size and complexity[2,20,21]. Logical strategies, such as sequential assembly or combinatorial coupling[21,22], can be readily imparted into microfluidic systems to control the spatial and temporal loading of functional modules. As the alternative, bulk methodologies require no specialized instruments and thus may recreate key scenarios during the emergence of life[23]. Additionally, synthetic cell architectures can be generated in super high yields using bulk methods to satisfy the demands for the industrial or medical application of synthetic cell products. However, current bulk methodologies are generally not able to produce lipid vesicles or coacervates with desired order and complexity. Firstly, bulk assembled cell-sized lipid vesicles or coacervates are almost always characterized by wide population size distributions[2], which is undesirable for applications that require quantifiability and reproducibility. Secondly, vesicles spontaneously assembled from lipids generally exhibit heterogenous lamellarity, failing to mimick the hallmark of cell envelope. Finally, although efforts have been made to add complexity in lipid vesicles or coacervates[24,25], it is still inaccessible to introduce logical strategies in bulk methodologies to control the spatial and temporal loading of building blocks for desired hierarchical complexity. The lack of control over the cellular order and complexity of vesicles and coacervates in general bulk assembly systems reinforces the puzzle about how inanimate matter have been properly integrated towards life and limits the application of synthetic cells in fields requiring yields, size uniformity, and flexibly integrated functions.

Here, we show that the interplay of colloidal particles with coacervate-forming molecules provides a mechanism for the bulk assembly of coacervates and lipid vesicles with controlled order and hierarchical complexity. Monodisperse coacervates stabilized by colloidal particles are generated via vortexing for tens of seconds. The complexity of coacervate entities is precisely and logically engineered via programmable combinatorial fusion or sequential loading, which enables further manipulation of coacervate entities into diverse interconnected coacervate consortia with emergent collective morphology evolution, thus providing an approach for the long-time goal[26] to integrate synthetic cells into a compartment hierarchy analogous to the organelle-cell-tissue structure of multicellular systems. Monodisperse giant unilamellar vesicles (GUVs) are generated by the freeze-thaw treatment of coacervates coated by liposome particles. Gated permeability to polar molecules and remarkable structural and functional stability at extreme environments are exhibited in these monodisperse lipid vesicles. The bulk methodology in this work represents as a possible approach for the proper integration of inanimate matter towards life and can be utilized for the on-demand

generation of high yields monodisperse coacervates and lipid vesicles with flexibly integrated functions to boost the application of synthetic cells.

Results and Discussion

Assembly colloidal particles with coacervate-forming molecues. The interplay of colloidal particles with coacervates is involved in the functioning of many biomolecular condensates[27,28], functionalization of coacervates for specific applications[24,29], and possibly emergence of protocellular life[30]. This work expolited a vortex assisted co-assembly method to systematicly investigate the interaction of colloidal particles with coacervates. Poly(diallyldimethylammonium chloride) (PDDA) and adenosine 5-triphosphate (ATP) were taken as model coacervate-forming molecues to assemble with various colloidal particles. PDDA and colloidal particles were firstly mixed, and then subsequently with ATP via vortex for 30 s. Depending on [PDDA] and [ATP] ratio φ and particle type, four cases were observed in the assembly results (Figs. 1a, b and S1, 2), namely, polydisperse coacervates with particles outside (Case 1), at interface (Case 2), or inside (Case 3), and monodisperse coacervates interfacially stabilized by particle layer (Case 4). Here, we demonstrated the bulk assembly of monodisperse coacervates (Case 4) for the first time. Various nanoparticles, including lipsomes with different membrane compositions, silica particles encompassed by lipid membrane, magnetic nanoparticles, and some polystyrene (PS) particles, are shown to be able to assemble with PDDA and ATP to form monodisperse coacervates (Fig. 1b and S3). The diameter of the coacervates can be controlled by varying the amount of liposomes used from several micrometers to tens of micrometers (Fig. S4). Stability test showed no obvious variation of their average diameter and morphology at 4^{o}C in three days (Fig. S5).

Mechanism of monodisperse coacervates formation. To elucidate the mechanisms for the different partitioning behaviors of particles across coacervates and the bulk formation of monodisperse coacervates, we use liposome as model particle and investigate the influence of liposome composition and [PDDA]/[ATP] ratio φ on coacervate formation. The φ and 1,2-dioleoyl-*sn*-glycero-3-phospho-L-serine (sodium salt) (DOPS) percentage χ in 1,2-dioleoyl-*sn*-glycero-3-phosphocholine (DOPC)/DOPS liposomes affect the formation of coacervates into the four cases in Fig. 1a, as indicated by the phase diagram in Fig. 1c. With an increase of φ or χ, liposomes display a partition tendency from the dilute phase (Case 1) to the interface (Case 2 and 4), and then to the coacervate phase (Case 3). Monodisperse coacervates are generated at χ value from 5% to 12% at specific φ range. With increasing χ, the range of φ shifts to a lower φ value.

Based on the results in Fig. 1c, we propose an interfacial tension determined partitioning mechanism for charged particles in coacervate system (Fig. 1d). A charged particle in the coacervate system is considered to exist as a complex comprising particle and adsorbed charged polymers. An interfacial tension $\gamma_{p\text{-}d}$ between particle-polymer complex and dilute phase appears because of particle-polymer charge complexation[31]. Analogous to particle partitioning in oil-water and aqueous two phase systems[32,33], the partitioning behavior of the particle-polymer complex is a result of the balance among $\gamma_{p\text{-}d}$, coacervate phase-dilute phase interfacial tension $\gamma_{c\text{-}d}$ and particle-coacervate phase interfacial tension $\gamma_{p\text{-}c}$. The particle located in dilute phase when $\gamma_{p\text{-}c}>\gamma_{p\text{-}d}+\gamma_{c\text{-}d}$ and in coacervate phase when $\gamma_{p\text{-}d}>\gamma_{p\text{-}c}+\gamma_{c\text{-}d}$. A contact angle θ with $\cos\theta=(\gamma_{p\text{-}c}-\gamma_{p\text{-}d})/\gamma_{c\text{-}d}$ is expected when the particle-polymer complex located at coacervate surface. With reference to Fig. 1c, an increase of χ would represent a strengthening of the association between liposome and PDDA, while an increase of φ

would induce more PDDA adsorption, thereby resulting in an increase of $\gamma_{p\text{-}d}$. Therefore, with the increase of χ and φ, the increased $\gamma_{p\text{-}d}$ induces the partition of liposomes from dilute phase to interface, and to coacervate phase. Based on the above mechanism, the zeta potential ζ of different charged colloidal particles should play a determining role in particle partitioning behavior. We test this hypothesis by characterizing the partitioning behaviors of different charged particles with diameter ranging from 30 nm to 100 nm in PDDA-ATP coacervates (φ=3/2). Particles with $|\zeta|$ below 10 mV, between 10 mV to 40 mV, or above 40 mV preferentially locate in the dilute phase, interface, or coacervate phase, respectively, in agreement with our hypothesis. The interfacial tension driven partitioning behavior might account for the various reported cargo recruitment behaviors in synthetic coacervates[30,34] and biomolecular condensates[27]. Besides, this mechanism built the foundation for the engineering of particle partitioning via tailoring particle surface properties. 100 nm silica particles with ζ of -52.3±4.1 mV positioned in the coacervate phase when assembled with PDDA and ATP (Fig. S2). However, when coated with DOPC/DOPS (χ=7.5% or 10%) lipid bilayer, their location shifts to the coacervate surface (Fig. S3).

A limited coalescence process promoted by vortexing is considered to acount for the formation of particle coated monodisperse PDDA-ATP coacervates (Fig. 1f). Small coacervates with particles on surface are firstly formed upon mixing of PDDA, particles and ATP. Because of the large specific surface area of these initially formed small coacervates, the particle coverage is too low to provide enough protection against coalescence. Therefore, driven by $\gamma_{c\text{-}d}$, these coacervates tend to coalesce under vortex, consequently reducing the coacervate specific surface area and increasing particle packing. Metastable coacervates are generated when the particle layer provided enough steric hindrance and repulsive electrostatic energy against further coalescence. The monodispersity of these particle-coated coacervates depended on φ, particle charges, and formation method (vortex or gentle incubation). φ and particle charges influenced the contact angle θ of particles on coacervate surface. To generate monodisperse coacervates, θ should be <90^o but large enough to avoid particle desorption during coalescence process. Comparing the vortexing and gentle incubation method (Fig. S6), vortexing promotes collision of the coacervates and overcomes the resistance of electrostatic repulsive forces among coacervates against coalescence, thus resulting in the formation of coacervates with remarkable monodispersity (Polydispersity index <0.02) in 30 s (Fig. 1g).

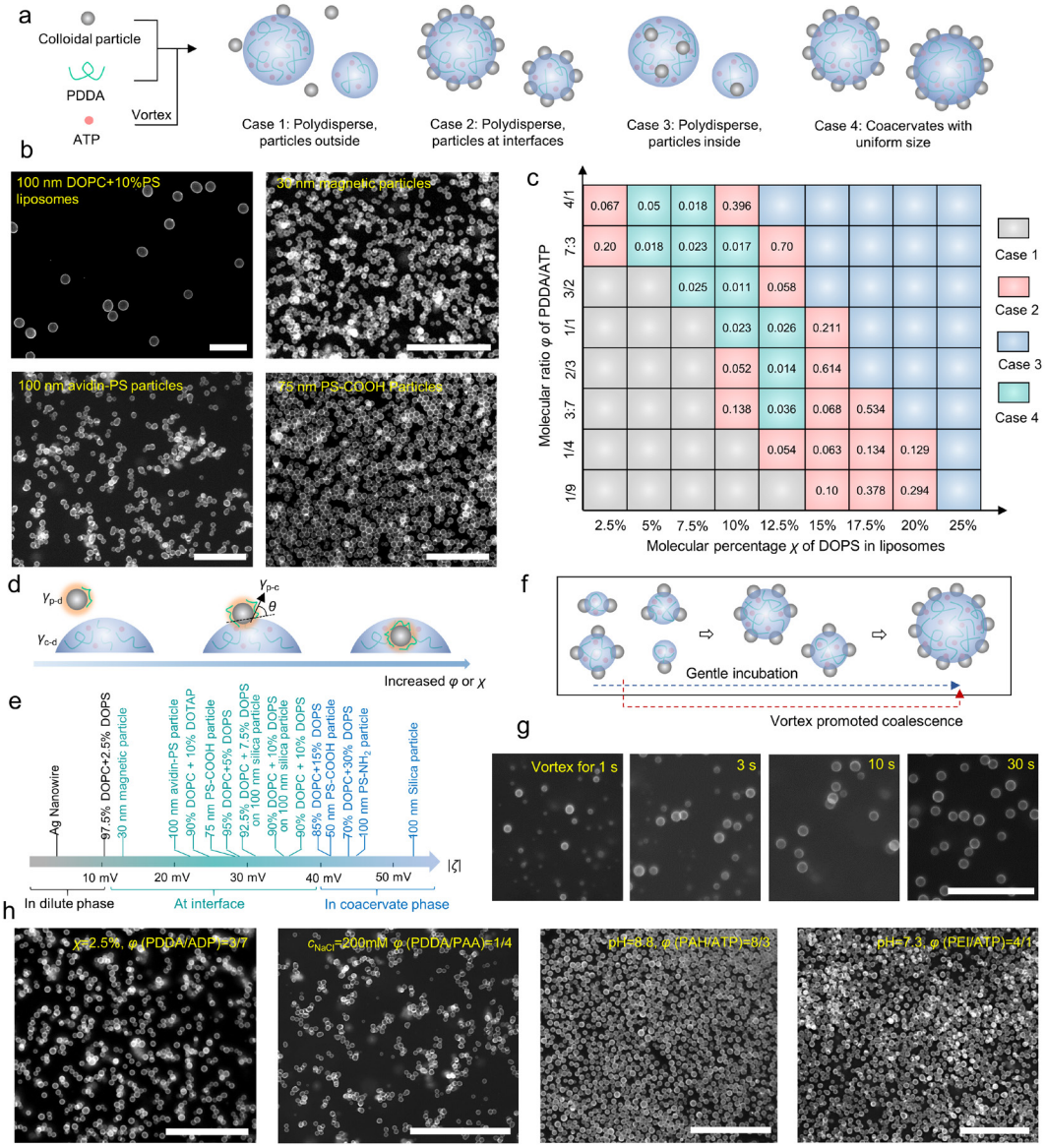

Figure 1. Formation of monodisperse coacervates a, Schematic showing four cases of the assembly results by mixing PDDA and colloidal particles firstly and subsequently with ATP via vortex. **b**, Fluorescence images of monodisperse coacervates coated by 100 nm DOPC/DOPS liposomes (Molecular percentage of DOPS χ = 10%), 30 nm magnetic nanoparticles, 100 nm streptavidin-coated PS particles, or 75 nm PS-COOH particles. [PDDA]+[ATP] concentration in final mixture was 5 mM. PDDA/ATP molecular ratio φ in the four colloids-coacervate systems were respectively 13:7, 1:1, 3:2, and 3:2. Colloids concentration were respectively 0.05, 0.035, 0.10, and 0.05 mg/mL. **c**, Phase diagram for the assembly results in DOPC/DOPS liposome-PDDA-ATP system at different χ and φ. The values in the table were the calculated polydispersity index from at least 100 coacervates for each case. Coacervate dispersion with polydispersity index $\leq$ 0.05 was considered as monodisperse. **d**, Schematic illustrating the mechanism of liposome partitioning across coacervate controlled by φ and χ. **e**, Positioning behavior of colloidal particles of different compositions and zeta potential $|\zeta|$ across PDDA-ATP coacervates (φ=3/2). **f**, Schematic showing the accelerated formation of metastable coacervates coated by colloidal particles from vortex assisted coalescence. **g**, Fluorescence images of the PDDA-ATP (φ=3/2) coacervates coated by DOPC/DOPS (χ = 10%) liposomes by vortexing for different time. Liposome concentration was 0.03 mg/mL. **h**, Fluorescence images of monodisperse coacervates formed from other charged species. Scale bars in b, g, and h were 50 μm.

Monodisperse coacervate formation from other charged species. To validate the versatility of this method to generate monodisperse coacervates with different components, DOPC/DOPS liposomes are used as model particles for co-assembly with another four cationic specie-anionic specie pairs, namely, PDDA with two anionic species, adenosine diphosphate (ADP) and polyacrylic acid (PAA), and ATP with two cationic species, polyallylamine (PAH) and polyethyleneimine (PEI). These four pairs represent typical examples with different degree of charge association in comparison with PDDA-ATP, following PDDA-PAA>PDDA-ATP>PDDA-ADP and PAH-ATP>PEI-ATP>PDDA-ATP at neutal pH condition.

Monodisperse coacervates are generated in all four different systems but under different conditions (Fig.1h and S7). In the PDDA-ADP system, monodisperse coacervates are generated at low χ value of 2.5% with φ (PDDA/ADP) ranging from 1/4 to 3/7 (Fig. S7a). In the PDDA-PAA system, no coacervates are formed in the absence of salt. Monodisperse PDDA-PAA coacervates coated by DOPC/DOPS (χ=50%) liposomes are obtained with NaCl concentration above 100 mM and φ (PDDA/PAA) range of 1/4 to 3/7 (Fig. S7b). In PAH-ATP and PEI-ATP systems,monodisperse coacervates are formed at alkaline pH condition when assembled with DOPC/DOPS (χ=10%) liposomes (Fig. S7c, d). Monodisperse PAH-ATP coacervates are formed at pH=8.8 and φ (PAH/ATP) range of 8/3 to 4/1 (Fig. S7c). PEI-ATP system needed a relative lower alkaline pH value from 7.3 to 7.7 and φ (PAH/ATP) range of 7/3 to 4/1 to generate monodisperse coacervates (Fig. S7d). The different requirements for the formation of monodisperse coacervates with different components can be explained by a balance among $\gamma_{p\text{-}c}$, $\gamma_{p\text{-}d}$ and $\gamma_{c\text{-}d}$, as shown in Fig.1d. For example, ADP was more weakly associated with PDDA than ATP, which resulted in smaller $\gamma_{c\text{-}d}$. Therefore, to avoid partitioning of liposomes in coacervate phase ($\gamma_{p\text{-}d}>\gamma_{p\text{-}c}+\gamma_{c\text{-}d}$), liposomes with low χ value of 2.5% that provide small $\gamma_{p\text{-}d}$ are used to stabilize coacervates (Fig. S7a). In contrast, with the more strongly associated PDDA-PAA, PAH-ATP and PEI-ATP systems (Larger $\gamma_{c\text{-}d}$), to generate monodisperse coacervates, salt concentration or pH value need to be modulated to reduce $\gamma_{c\text{-}d}$, or alternatively, liposomes with higher χ are used to increase $\gamma_{p\text{-}d}$.

Hierarchical coacervates via combinatorial fusion. Very small unstable coacervates were firstly formed when particles and counter-charged species were just mixed, which took more than 30 min for them to fuse into metastable coacervates through gentle incubation, but only 30 s via vortexing, as shown in Fig. 1f, g and S6. This difference implies the potential to engineer the hierarchical coacervates via combinatorial fusion. A series of small unstable coacervates with various structures were first formed via the gentle mixing of particles and counter-charged species. These small coacervates are then taken as building blocks to generate hierarchical coacervates with elaborately engineered structures via vortex-assisted fusion of selected building blocks.

Nine types of coacervate building blocks (1)-(9) are designed by gently mixing PDDA, ATP, liposomes with red (R-liposome) or green (G-liposome) fluorescence, PAH, or PS particles with blue (B-PS particle) or green (G-PS particle) fluorescence (Fig. 2a). Through the self- or mutual fusion of these building blocks via vortexing, the surface and inner compartment of the coacervates can be elaborately engineered. On PDDA-ATP coacervate surface, the spatial organization of R-liposome and G-liposome can be controlled, including the heterogeneously distributed configuration comprising microsized patches of different liposomes (Fig. 2b and S8) and homogeneous liposome mixing (Fig. 2c). Inside PDDA-ATP coacervates, the homogeneous or heterogenous spatial organization of one or two objects is delicately controlled (Fig. 2d-g).

Multiphase coacervates composed of PDDA-ATP rich phase and PAH-ATP rich phase (Fig. 2h and S9) are generated via the vortex-assisted self-fusion of coacervate building blocks (7); the resultant morphology bears resemblance to those of eukaryotic cells with inner phase as nucleus and outer phase as cytoplasm. An even higher degree of complexity can be introduced into these multiphase coacervates by spatial loading of B-PS particle or G-PS particle in PDDA-ATP-rich phase as "organelles" (Fig. 2i-j) through the self-fusion of building blocks (8) or (9). This combinatorial fusion approach provides a route for on-demand generation of coacervates with desired hierarchical structures.

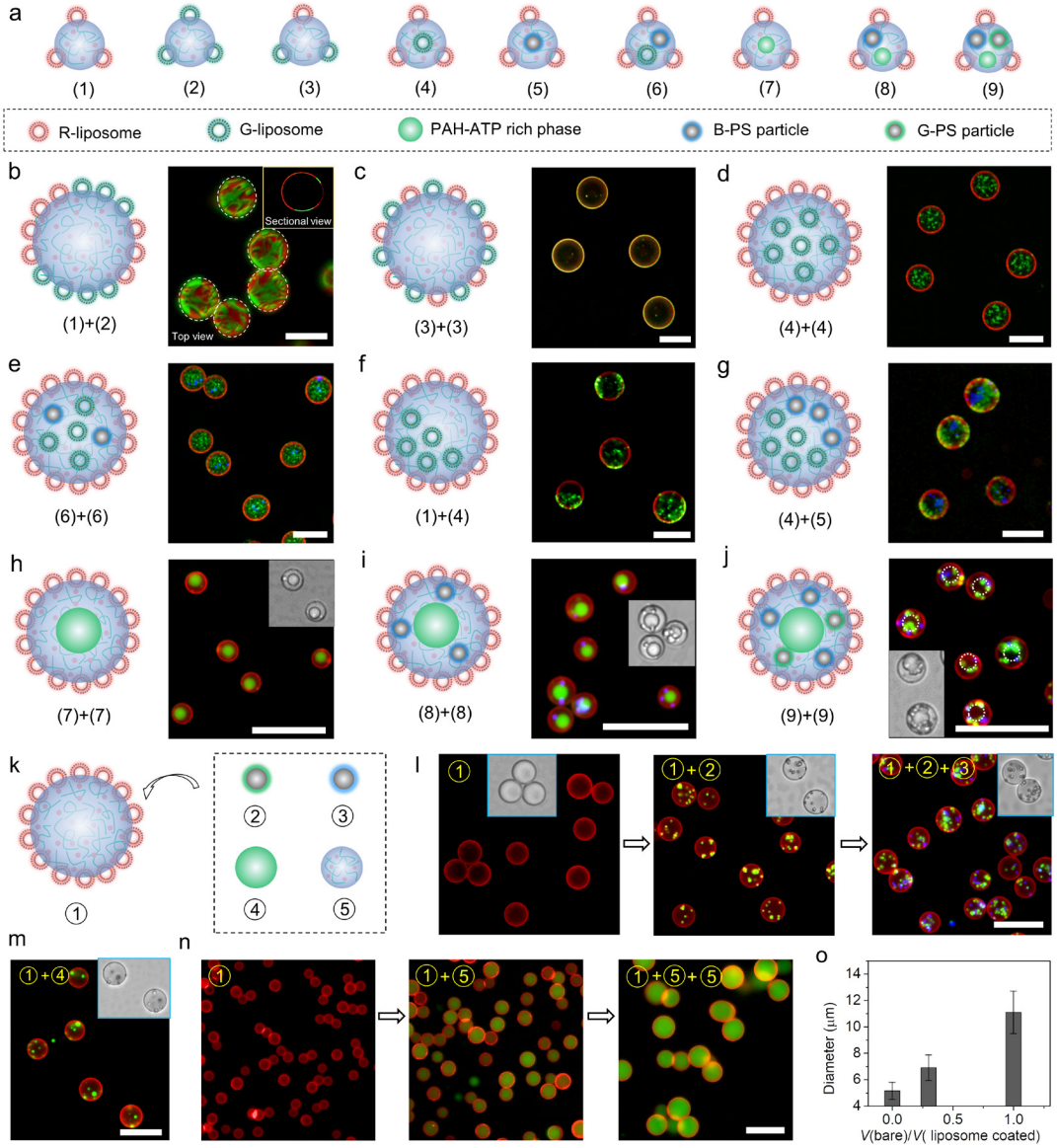

Figure 2. Combinatorially engineering the hierarchy of coacervates. a-j, Engineering hierarchical coacervates via combinatorial fusion of small coacervate building blocks. **a**, Schematic of the nine small coacervate building blocks (1)-(9) formed via the gentle mixing of PDDA, ATP, PAH or different particles for combinatorial fusion experiments. R-liposome and G-liposome indicate liposomes with respectively red and green fluorescence. B-PS particle and G-PS particle indicate PS particles with respectively blue and green fluorescence. **b-j**, Schematic and fluorescence images of various hierarchical coacervates formed via vortex promoted fusion of coacervate building blocks from **a**. **k-o**, Sequential loading of different cargos into liposome particles stabilized coacervates. k, Schematic

illustrating the sequential loading G-PS particle ②, B-PS particle ③, PAH-ATP rich coacervate ④, or bare PDDA-ATP coacervate with FITC-PLL inside ⑤, into the R-liposome stabilized coacervates ①. **l**, Fluorescence and inset bright field images showing the sequential loading of ② and ③ into ①. **m**, fluorescence and inset bright field images of the multiphase coacervates with PAH-ATP rich inside formed via the loading of ④ into ①. **n**, fluorescence images showing volume growth of liposome stabilized coacervates via the loading of bare coacervates with 30% volume of ① (middle image) and 100% volume of ① (image at the right side). **o**, relationship of the calculated diameter of the final liposome stabilized coacervates with the volume of added bare coacervates from 100 coacervates for each event. The error bar represents the standard deviation. The scales bars were 20 μm.

Sequential loading and volume growth of particle stabilized coacervates. Besides the combinatorial fusion approach, the hierarchy of coacervates can also be engineered via post- loading (Fig. 2k). PDDA-ATP coacervates (φ=3/2) stabilized by DOPC/DOPS liposomes (χ=10%) are used as the starting structure to perform post-loading experiments, where the coacervates are mixed with different particles or bare coacervates, followed by subsequent vortexing for 10 s. G-PS particle and B-PS particles are shown to be sequentially loaded into the liposome coated coacervates (Fig. 2l). PAH-ATP coacervates can be sequestered to generate multiphase coacervates (Fig. 2l). Moreover, bare PDDA-ATP coacervates can also be sequenstered into liposome coated PDDA-ATP coacervates, leading to their volume growth to defined size (Fig. 4n-o). The sequential loading behaviors might imply a possible predatory behavior for protocellular life in the form of particle coated coacervate droplets to engulf other materials or bare coacervates for funtion evolution or volume growth. The combinatorial fusion and sequential loading represent two logical strategies to engineer coacervates towards specific hierarchical complexity.

Programmable assembly of tissue-like assemblages. The emergence of multicellularity represented a major transition in the evolution of life[35], which stimulated the recent trend to build synthetic multicellular systems with emergent properties from protocell entities, such as aqueous droplets in oil[36], proteinosomes[12], and liposomes[9]. However, the inherent difficulty to control adhesion of coacervates without fusion hamper the assembly of coacervats into muticellular assemblages. Here, taking advantage of the metastable hierarchical coacervates through combinatorial fusion or sequential loading, we demonstrate a method to program the assembly of interconnected coacervate consortia via tailoring coacervate structure. Six kinds of PDDA-ATP coacervates I-VI with different spatial organization of liposomes, magnetic particles, avidin-PS particles or PAH-ATP rich phase are prepared for coacervate assemblage formation (Fig. 3a). DOPC/DOPS (χ=10%) liposome-coated coacervates (Coacervates I), DOPC/DOPS (χ=10%) liposome-coated coacervates with 1 μm magnetic particle inside (Coacervates II), and 30 nm magnetic nanoparticle-coated coacervates (Coacervates III) exhibit non-specific aggregation into irregular clusters or magnetotactic bacteria-like aligned coacervate chains with embedded magnetic particle chains (Inset in Fig. 3b) after the application of external stimuli (pH or magnetic field); the consequent aggregation of coacervates I and II is reversible (Fig.3b). Specific aggregation was observed in coacervates IV (90% DOPC+10% biotin-lipid liposome coated coacervate) and V (Avidin-PS nanoparticle coated coacervates). Coacervates IV (Red fluorescence) and 1 μm avidin-PS particles (Green fluorescence) specifically associated into coacervate assemblage containing one coacervate type (Fig. 3c). More complicated coacervate assemblage containing two coacervate types IV (Red fluorescence) and V (Green fluorescence) can be formed via the specific association of the

biotin group in coacervate IV and the avidin group in coacervate V (Fig. 3d).

To form tissue-like coacervate assemblages at millimeter scale, we impose a magnetic field gradient on the top surface of a magnet (100mm×50mm×5mm) to guide the assembly of coacervates III or VI that have been coated by a mixture of magnetic nanoparticles and liposomes with different fluorescence (Lipid/Fe mass ratio=α). Strip-shaped coacervate assemblages with parallelly or serially coded patterns are generated via simultaneous or successive assembly of coacervate III (α=1/4) with respective red and green fluorescence as shown in Fig. 3f-h. Multiphase coacervates VI (α=4/1) are assembled using same method into tissue-like assemblage with excess complexity (Fig. 3i). Coacervates in the strip-shaped assemblages are interconnected and exhibit collective deformation or motion such as rotation, translation, folding and unfolding under magnetic field (Fig. S10). Moreover, diffusion-related morphology evolution is observed in coacervate III assemblage when 50 mM ATP is added from the right side of the assemblage (Fig. 3g). The high concentration of ATP induces desoprtion of the liposomes from coacervates (Inset schematic in Fig. 3g and Fig. S11). Therefore, coacervates fuse into defined size depending on α for a new magnetic particle steric hindrance layer (Inset schematic in Fig. 3g and Fig. S12). With ATP diffusion, fusion events sweep from right to left (Fig.3g). These results indicated the ability of the coacervate assemblage to exhibit collective behavior in response to physical or chemical stimuli.

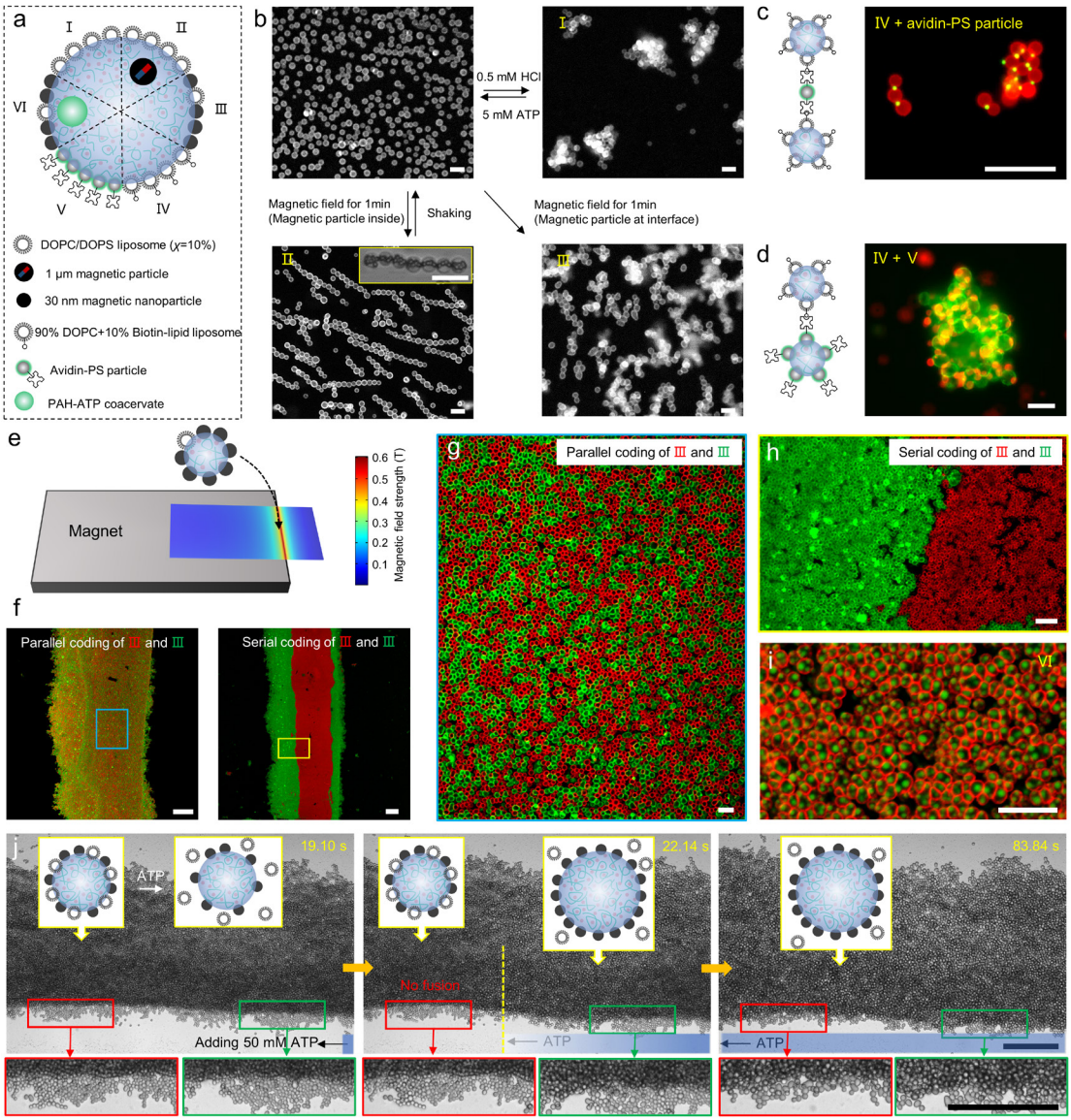

Figure 3. Assembly of coacervates into tissue-like assemblages and their collective behavior. a, Schematic of the six kinds of coacervates for coacervate assemblage formation. **b**, PDDA-ATP coacervate assemblage formation via non-specific interaction of coacervates I-III respectively. The inset was a bright field image of coacervate assemblage formed from coacervate II. **c**, Schematic and merged fluorescence image showing the specific aggregation of red fluorescent coacervate IV linked by 1μm green fluorescent avidin-PS particle. **d**, Schematic and merged fluorescence image showing the specific association of coacervates IV (red fluorescence) and V (green fluorescence). **e**, Simulated magnetic field distribution on one side of the 100mm×50mm×5mm magnet top surface. **f**, Fluorescence images of the coacervates assemblages via the parallel (left) and serial (right) coding of coacervates III with respective red and green fluorescence. **g** and **h**, Enlarged images of the parallelly (**g**) and serially (**h**) coded coacervates assemblages in the white box in **f**. **i**, Merged fluorescence image of the coacervate assemblage formed from coacervate VI. **j**, Collective fusion of coacervates III in the assemblage after the addition of 5 μL ATP stock solution from the right side of the assemblage. The inset in the left image was a schematic showing the shedding of liposomes after adding ATP. The inset in the middle and right images were schematic showing the structure of the coacervates at position directed by the arrows. The molecular ratio α of lipid and Fe was 1/1. Scale bars in **b-d** and **g-i** were 10 μm. Scale bars in **f** and **j** were 200 μm.

Bulk assembly of monodisperse GUVs. Biological cells are bounded with phospholipid membranes separating the intracellular and extracellular space. The assembly of phospholipid membrane on coacervates represents a further step to construct synthetic cells with both hallmarks of cell envelope and cytoplasm and may bridge the gap between coacervate-based protocell models and membrane bounded biological cells. Bare coacervates have recently been utilized templates to incubate with lipids in ethanol or hydrated lipid film, resulting in polydisperse giant phospholipid vesicles with apparent lamellarity[37,38]. In this work, through the freeze-thaw treatment of monodisperse coacervates coated by DOPC/DOPS/Chol (37/3/10) liposomes, we demonstrate the first example for the bulk assembly of monodisperse GUVs (Fig. 4).

Fluorescein is used as the probe to check the permeability of the coacervate-supported GUVs formed through freeze-thaw method (Fig. 4b). Recent work indicated that coacervate-supported phospholipid membrane contained defects and thus was leaky[37]. Here, we show that the membrane permeability of coacervate-supported GUVs can be tunable. With PDDA in dispersion media, GUVs are leaky and can enrich fluorescein in coacervate nucleus, probably due to the transient membrane defects from PDDA adsorption. When PDDA is removed by washing with excess 5 mM ATP solution, membrane permeability to fluorescein is blocked. As no sophisticated protein machinery is involved, the gated permeability of membrane on coacervates might provide a primitive approach for tunable cargo transportation across the membrane barrier of protocells. Membrane unilamellarity is confirmed by the enrichment of fluorescein after incubating the coacervate-supported GUVs with melittin (Right image in Fig. 4b). Fluidity of membrane is confirmed by fluorescence recovery after photobleaching (FRAP) experiments (Fig. 4c). The coacervate nucleus inside the GUVs is verified by the phase contrast images (Inset in Fig. 4b) and FRAP experiment (Fig. 4d).

The freezing conditions (-196ºC in liquid nitrogen, -80ºC or -20ºC) were found to influence the size distribution of coacervate-supported GUVs and their formation efficiency from coacervates coated by liposome particles (Fig. S13). Quicker freezing at lower temperature resulted in better monodispersity and higher transformation efficiency. By using liquid nitrogen for freezing, a transformation efficiency of above 50% to monodisperse GUVs with PDI value of 0.014 can be achieved (Fig. S13). The average size of the coacervate-supported GUVs can be controlled by varying lipid concentration in the dispersion of the coacervates coated by liposome particles. With lipid concentration increasing from 0.015 mg/mL to 0.05 mg/mL, the average diameter decreased from ~8 μm to ~2 μm (Fig. 4e, f). The lamellarity of the coacervate-supported giant vesicles was influenced by the property of the liposome particles for coacervate stabilization. When multilamellar liposome particles were utilized, multilamellar membrane was formed on coacervates (Fig. S14). However, when only 33.3 wt% of unilamellar liposomes were co-assembled with multilamellar liposomes on coacervate surface, a proportion of above 85% for GUVs was generated in the obtained assemblies (Fig. S14), which indicated the possible role of this approach to regularize prebiotic lipid vesicles with heterogenous lamellarity towards unilamellar protocellular structures. The release of the coacervate nucleus to form non-supported GUVs was realized by incubating the coacervate-supported GUVs in solution media with 150 mM NaCl and 0.5 μg/mL melittin (Fig. S15). The non-supported GUVs displayed active membrane fluctuations and exhibited a morphology evolution towards lipid tubes under hypertonic conditions.

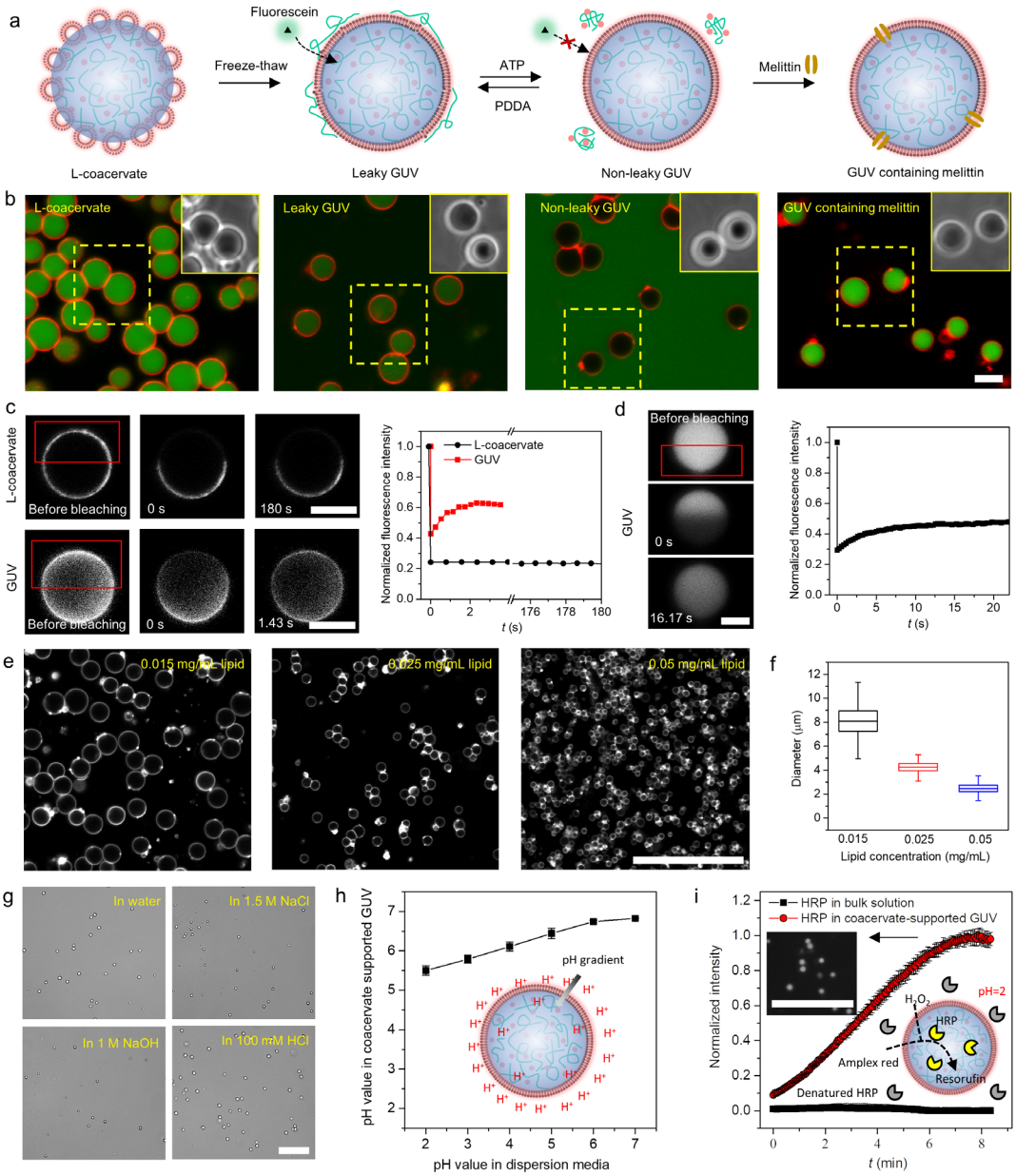

Figure 4. Assembly of monodisperse GUVs with tunable permeability and remarkable structural and functional integrity at extreme environments. a, Schematic illustrating the formation and permeability of DOPC/DOPS/Chol (37/3/10) GUVs on PDDA-ATP coacervates (φ=7/3) from liposome coated coacervates (L-coacervate). **b**, Fluorescence images showing the permeability to fluorescein of L-coacervate, leaky GUV, Non-leaky GUV, and GUV containing melittin. The inset were the phase contrast images of droplets in the yellow dash boxes. The sample was frozen in liquid nitrogen. **c**, Fluorescence recovery after photobleaching (FRAP) experiments of rhodamine-DOPE in L-coacervate and GUV. **d**, FRAP experiment of FITC-PLL inside GUV. **e** and **f**, Size control of GUVs formed via freeze in liquid nitrogen. The error bar represents the standard deviation. For all cases, n>100. **g**, Bright field images of coacervate-supported GUVs at extreme environments. **h**, Apparent pH value in coacervate supported GUVs versus pH value in dispersion media. A pH gradient was generated as shown by the inset schematic. **i**, Enzyme catalyzed reaction in bulk solution and coacervate supported GUVs at pH=2. The inset was the schematic and a typical fluorescence image showing the generation of resorufin in coacervate supported GUVs. The error bars represent the standard error of mean (SEM), n = 3 independent experiments. Scale bars in **b**-**d** were 5 μm. Scale bars in **e**, **g**, **i** were 50 μm.

Structural and functional stability of coacervate-supported GUVs at extreme environments. Turbidity tests were performed to check the stability of the PDDA-ATP coacervate-supported GUVs at different salt concentrations or pH conditions (Fig. S16). Bare PDDA-ATP coacervates are shown to readily dissociated at NaCl concentration above 50 mM, acid condition with pH value below 3, and alkaline condition with NaOH concentration above 100 mM. However, no obvious turbidity change was observed for coacervate-supported GUVs in the investigated NaCl concentration range between 0-1.6 M, acid condition with pH value to 2, and alkaline condition with NaOH concentration to 1 M. Moreover, bright field images showed that these coacervate-supported GUVs retained their spherical morphology at such extreme osmotic, salty, acidic, or alkaline conditions (Fig. 4g), which indicated their remarkable structural stability.

Non-supported GUVs and coacervates were both very sensitive to osmosis, salt concentration or pH value[10]. However, the integrated form of these two compartments, coacervate-supported GUVs, displayed unexpected acid-, alkali-, salt-, and osmosis- resistance ability. Here, we attributed to the structural stability towards salt and osmosis to the synergistic effects of the membrane and coacervate nucleus. Phospholipid membrane functioned as a barrier to ions, thus protecting the salt-sensitive coacervate nucleus from incompatible salt concentration. In turn, the repulsive molecular forces inside coacervates and the viscosity of coacervates provided a hydrostatic pressure against water loss[9], thus resulting in the insensitivity of the vesicular coat to osmosis.

The pH stability of the coacervate-supported GUVs might be because the coacervate nucleus served as buffer to provide a relatively stable local pH condition. To address this question, we used pH-sensitive FITC-PLL as probe, which has showed high partition coefficient into coacervate phase (Fig. S17), to measure the apparent pH value inside coacervates. As shown in Fig. 4h, the coacervate nucleus kept a pH value between 5.5 to 7 when pH value outside varies from 2-7 (Fig. 4h), which consistent with the anticipated role of coacervate nucleus as the buffer. This effect on one hand enabled the generation of a transmembrane pH gradient, which might be involved in the evolution and biosynthesis of prebiotic life[39]. On the other hand, it provided a pH homeostatic environment for biomolecules. We showed that the pH homeostasis enabled the functioning of horseradish peroxidase (HRP) inside the coacervate-supported GUVs to transform amplex red into red fluorescent resorufin at an extreme pH value of 2 that was able to denature enzymes (Fig. 4i). This structural and functional stability may enable the survival and functioning of primitive life at extreme conditions. Besides, it may also render them as robust synthetic cells to replace the fragile biological cells for specific functions.

Conclusion

In summary, this work paved an unprecedented step to form monodisperse, hierarchical coacervate droplets and GUVs as synthetic cells without using specialized microfluidic devices. The hierarchical complexity of the synthetic cell architectures was delicately engineered from the spatial or temporal organization of different components in single synthetic cell entity, to manifold forms of interconnected synthetic cell consortia. The increased hierarchical complexity gave rise to emergent properties in the synthetic cell systems, for instance, the collective morphology evolution of coacervate assemblages, and the remarkable structural and functional stability of the coacervate-supported GUVs. This work provides a prebiotically plausible approach for inanimate matter to get their proper order and complexity towards primitive life. The logical strategies in this work, such as combinatorial fusion or sequential loading, are promisingly utilized in labs as high throughout

integrative approaches to explore the possibly integrated form of life from a high diversity of inanimate matter. Moreover, the bulk assembly nature of this methodology enables the high yields generation of monodisperse synthetic cell compartments with flexibly integrated components or functions, which can be widely applied in follow-up scientific and technological applications, such as the study of cell working principles, the fabrication of living materials, microreactors, and biosensors, and the developments of underwater adhesive or advanced delivery systems.

References

1 Schwille, P. Bottom-Up Synthetic Biology: Engineering in a Tinkerer's World. *Science* **333**, 1252-1254, doi:10.1126/science.1211701 (2011).

2 Ugrinic, M., deMello, A. & Tang, T. Y. D. Microfluidic Tools for Bottom-Up Synthetic Cellularity. *Chem* **5**, 1727-1742, doi:https://doi.org/10.1016/j.chempr.2019.03.012 (2019).

3 Adamala, K. & Szostak, J. W. Nonenzymatic Template-Directed RNA Synthesis Inside Model Protocells. *Science* **342**, 1098-1100, doi:10.1126/science.1241888 (2013).

4 Vutukuri, H. R. *et al.* Active particles induce large shape deformations in giant lipid vesicles. *Nature* **586**, 52-56, doi:10.1038/s41586-020-2730-x (2020).

5 Peters, R. J. *et al.* Cascade reactions in multicompartmentalized polymersomes. *Angewandte chemie* **126**, 150-154 (2014).

6 Liu, S. *et al.* Enzyme-mediated nitric oxide production in vasoactive erythrocyte membrane-enclosed coacervate protocells. *Nature Chemistry* **12**, 1165-1173, doi:10.1038/s41557-020-00585-y (2020).

7 Buddingh', B. C. & van Hest, J. C. M. Artificial Cells: Synthetic Compartments with Life-like Functionality and Adaptivity. *Accounts of Chemical Research* **50**, 769-777, doi:10.1021/acs.accounts.6b00512 (2017).

8 Zhu, T. F. & Szostak, J. W. Coupled Growth and Division of Model Protocell Membranes. *Journal of the American Chemical Society* **131**, 5705-5713, doi:10.1021/ja900919c (2009).

9 Li, Q., Li, S., Zhang, X., Xu, W. & Han, X. Programmed magnetic manipulation of vesicles into spatially coded prototissue architectures arrays. *Nature Communications* **11**, 232, doi:10.1038/s41467-019-14141-x (2020).

10 Zong, W. *et al.* A Fissionable Artificial Eukaryote-like Cell Model. *Journal of the American Chemical Society* **139**, 9955-9960, doi:10.1021/jacs.7b04009 (2017).

11 Rideau, E., Dimova, R., Schwille, P., Wurm, F. R. & Landfester, K. Liposomes and polymersomes: a comparative review towards cell mimicking. *Chemical Society Reviews* **47**, 8572-8610, doi:10.1039/C8CS00162F (2018).

12 Gobbo, P. *et al.* Programmed assembly of synthetic protocells into thermoresponsive prototissues. *Nature Materials* **17**, 1145-1153, doi:10.1038/s41563-018-0183-5 (2018).

13 Rodríguez-Arco, L., Li, M. & Mann, S. Phagocytosis-inspired behaviour in synthetic protocell communities of compartmentalized colloidal objects. *Nature Materials* **16**, 857-863, doi:10.1038/nmat4916 (2017).

14 Chen, H. *et al.* Fusion-Induced Structural and Functional Evolution in Binary Emulsion Communities. *Angewandte Chemie International Edition* **59**, 16953-16960, doi:https://doi.org/10.1002/anie.202004617 (2020).

15 Mason, A. F., Buddingh', B. C., Williams, D. S. & van Hest, J. C. M. Hierarchical Self-Assembly of a Copolymer-Stabilized Coacervate Protocell. *Journal of the American Chemical Society* **139**,

17309-17312, doi:10.1021/jacs.7b10846 (2017).

16 Abbas, M., Lipiński, W. P., Wang, J. & Spruijt, E. Peptide-based coacervates as biomimetic protocells. *Chemical Society Reviews*, doi:10.1039/D0CS00307G (2021).

17 Poudyal, R. R. *et al.* Template-directed RNA polymerization and enhanced ribozyme catalysis inside membraneless compartments formed by coacervates. *Nature Communications* **10**, 490, doi:10.1038/s41467-019-08353-4 (2019).

18 Dora Tang, T. Y. *et al.* Fatty acid membrane assembly on coacervate microdroplets as a step towards a hybrid protocell model. *Nature Chemistry* **6**, 527-533, doi:10.1038/nchem.1921 (2014).

19 Deshpande, S. *et al.* Spatiotemporal control of coacervate formation within liposomes. *Nature Communications* **10**, 1800, doi:10.1038/s41467-019-09855-x (2019).

20 van Swaay, D., Tang, T. Y. D., Mann, S. & de Mello, A. Microfluidic Formation of Membrane‐Free Aqueous Coacervate Droplets in Water. *Angewandte Chemie* **127**, 8518-8521 (2015).

21 Weiss, M. *et al.* Sequential bottom-up assembly of mechanically stabilized synthetic cells by microfluidics. *Nature Materials* **17**, 89-96, doi:10.1038/nmat5005 (2018).

22 Bawazer, L. A. *et al.* Combinatorial microfluidic droplet engineering for biomimetic material synthesis. *Science Advances* **2**, e1600567, doi:10.1126/sciadv.1600567 (2016).

23 Ghosh, B., Bose, R. & Tang, T. Y. D. Can coacervation unify disparate hypotheses in the origin of cellular life? *Current Opinion in Colloid & Interface Science*, 101415, doi:https://doi.org/10.1016/j.cocis.2020.101415 (2020).

24 Mason, A. F. *et al.* Mimicking Cellular Compartmentalization in a Hierarchical Protocell through Spontaneous Spatial Organization. *ACS Central Science* **5**, 1360-1365, doi:10.1021/acscentsci.9b00345 (2019).

25 Trantidou, T. *et al.* Engineering Compartmentalized Biomimetic Micro- and Nanocontainers. *ACS Nano* **11**, 6549-6565, doi:10.1021/acsnano.7b03245 (2017).

26 Göpfrich, K., Platzman, I. & Spatz, J. P. Mastering Complexity: Towards Bottom-up Construction of Multifunctional Eukaryotic Synthetic Cells. *Trends in Biotechnology* **36**, 938-951, doi:https://doi.org/10.1016/j.tibtech.2018.03.008 (2018).

27 Milovanovic, D., Wu, Y., Bian, X. & De Camilli, P. A liquid phase of synapsin and lipid vesicles. *Science* **361**, 604-607, doi:10.1126/science.aat5671 (2018).

28 Fujioka, Y. *et al.* Phase separation organizes the site of autophagosome formation. *Nature* **578**, 301-305, doi:10.1038/s41586-020-1977-6 (2020).

29 Pavan Kumar, B. V. V. S. *et al.* Chloroplast-containing coacervate micro-droplets as a step towards photosynthetically active membrane-free protocells. *Chemical Communications* **54**, 3594-3597, doi:10.1039/C8CC01129J (2018).

30 Koga, S., Williams, D. S., Perriman, A. W. & Mann, S. Peptide–nucleotide microdroplets as a step towards a membrane-free protocell model. *Nature Chemistry* **3**, 720-724, doi:10.1038/nchem.1110 (2011).

31 Spruijt, E., Sprakel, J., Cohen Stuart, M. A. & van der Gucht, J. Interfacial tension between a complex coacervate phase and its coexisting aqueous phase. *Soft Matter* **6**, 172-178, doi:10.1039/B911541B (2010).

32 Shi, S. & Russell, T. P. Nanoparticle Assembly at Liquid–Liquid Interfaces: From the Nanoscale to Mesoscale. *Advanced Materials* **30**, 1800714, doi:https://doi.org/10.1002/adma.201800714 (2018).

33 Song, Y. *et al.* Fabrication of fibrillosomes from droplets stabilized by protein nanofibrils at all-aqueous interfaces. *Nature Communications* **7**, 12934, doi:10.1038/ncomms12934 (2016).

34 Pir Cakmak, F., Grigas, A. T. & Keating, C. D. Lipid Vesicle-Coated Complex Coacervates. *Langmuir* **35**, 7830-7840, doi:10.1021/acs.langmuir.9b00213 (2019).

35 Grosberg, R. K. & Strathmann, R. R. The Evolution of Multicellularity: A Minor Major Transition? *Annual Review of Ecology, Evolution, and Systematics* **38**, 621-654, doi:10.1146/annurev.ecolsys.36.102403.114735 (2007).

36 Villar, G., Graham, A. D. & Bayley, H. A Tissue-Like Printed Material. *Science* **340**, 48-52, doi:10.1126/science.1229495 (2013).

37 Pir Cakmak, F., Marianelli, A. M. & Keating, C. D. Phospholipid membrane formation templated by coacervate droplets. *bioRxiv*, 2021.2002.2017.431720, doi:10.1101/2021.02.17.431720 (2021).

38 Zhang, Y. *et al.* Giant Coacervate Vesicles As an Integrated Approach to Cytomimetic Modeling. *Journal of the American Chemical Society*, doi:10.1021/jacs.0c12494 (2021).

39 Liu, L. *et al.* Enzyme-free synthesis of natural phospholipids in water. *Nature Chemistry* **12**, 1029-1034, doi:10.1038/s41557-020-00559-0 (2020).

Methods

Co-assembly of colloidal particles with coacervate-forming molecules

PDDA and ATP was taken as a pair of model coacervate-forming molecules to assemble with colloidal particles. PDDA stock solution (50 mM, V_1), colloidal particle dispersion (V_2), and water (V_3) were mixed firstly, and then subsequently with ATP stock solution (50 mM, V_4) via vortexing for 30 s to form the colloidal particles-coacervates hybrid system. The sum of V_1, V_2, V_3 and V_4 was 100 μL. V_1 + V_4 was 10 μL. $V_1/V_2=\varphi$ was the molecular ratio of PDDA and ATP. Assembly results (Partitioning behavior of particles and size distribution of coacervates) were characterized using fluorescence microscope. The influences of particle types, concentration and φ were investigated. To investigate the influence of coacervate composition on assembly results, assembly experiments of DOPC/DOPS liposomes with another four cationic specie-anionic specie pairs, namely, PDDA with two anionic species, ADP and PAA, and ATP with two cationic species, PAH and PEI, were further performed.

Hierarchical coacervates formation via combinatorial fusion

Below molecules or particles were used in the combinatorial fusion experiments: PDDA, ATP, three kinds of liposomes, namely, DOPC/DOPS (χ=10%) liposome with red fluorescence, DOPC/DOPS (χ=10%) liposome with green fluorescence and DOPC/DOPS (χ=50%) liposome with green fluorescence, and two kinds of PS particles, namely, 0.5 μm PS-COOH particle with green fluorescence and 1 μm PS-COOH particle with blue fluorescence. A series of coacervate precursors as building blocks were prepared by mixing PDDA with liposomes, other colloidal particles, or PAH firstly, and then gently mixing with ATP. In the dispersion of each coacervate precursor, the total concentration of cationic species was 3 mM, ATP concentration was 2 mM, the concentration of DOPC/DOPS (χ=10%) liposome was 0.015 mg/mL and the total volume of the dispersion was 100 μL. These coacervate precursors were combinatorically mixed and then vortexed for 30 s to generate coacervates with different hierarchical structures.

Sequential loading in coacervates coated by liposome particles

DOPC/DOPS (χ=10%) liposomes stabilized PDDA-ATP coacervates (φ=3/2) were formed via vortex. 0.5 μm PS-COOH particle with green fluorescence, 1 μm PS-COOH particle with blue fluorescence, bare PAH-ATP coacervates (φ(PAH/ATP) =1/1) with FITC-PAH inside or bare PDDA-ATP coacervates (φ=3/2) with FITC-PLL inside were added in the liposomes stabilized coacervates dispersion. The mixture was then vortexed for 10 seconds. The positioning of particles or bare coacervates and the volume variation of the liposomes stabilized coacervates were characterized using the fluorescence microscope.

Assembly of coacervates into tissue-like coacervates assemblages

Six kinds of coacervates with different components at interfaces or inside were prepared via vortex, including DOPC/DOPS (χ=10%) liposomes coated PDDA-ATP coacervates (φ=3/2) without (I) or with (II) 1 μm magnetic particle inside, PDDA-ATP coacervates coated by mixture of 30 nm magnetic particles and DOPC/DOPS (χ=10%) liposomes without (III) or with (φ(PDDA/PAH/ATP)=1/1/2) (VI) PAH-ATP rich phase inside, 90% DOPC+10% biotin-lipid liposome coated coacervate (φ=3/2) (IV), and 100 nm avidin-PS particle coated coacervates (φ=3/2) (V). These six kinds of coacervates were taken as building blocks to fabricate tissue-like coacervates assemblages through non-specific or specific association. External stimulus, such as pH value, ATP concentration or magnetic field, were used to guide the assembly. The specific association of coacervates IV or V was carried out by the gentle shaking of the mixture of coacervate IV and 1 μm avidin-PS particle or the mixture of coacervate IV and V on a shaking table for 1 h. To form coacervate assemblages from massive coacervates with defined morphology and spatial organization, the gradient magnetic field at the edge of the magnet top surface was utilized to guide the assembly of magnetic nanoparticles stabilized coacervates III and VI. A coverslip was placed on one side of the top surface of the magnet (100mm×50mm×5mm). Dispersions of magnetic nanoparticles stabilized coacervates were then simultaneously or successively placed on the coverslip to allow the formation of belt-shaped coacervate assemblages guided by magnetic field. Magnetic field distribution was simulated using the COMSOL Multiphysics 4.4 software.

GUVs formation on coacervates

Monodisperse PDDA-ATP Coacervates (φ=7/3) coated by DOPC/DOPS/Chol (molecular ratio=37/3/10) liposomes (L-coacervates) was firstly formed via vortex forced co-assembly process. The L-coacervates were frozen under liquid nitrogen, -80ºC or -20ºC and then thawed at room temperature to generate GUVs supported by coacervates. To guarantee size uniformity of the GUVs, L-coacervates formed with liposome concentration of 0.025 mg/mL and 0.05 mg/mL were diluted for three times before freezing. GUVs formation efficiency from L-coacervates was calculated by measuring the turbidity difference when dispersing the sample in water or 150 mM NaCl solution. The permeability of the coacervates to fluorescein was checked using fluorescence microscope. Membrane unilarmellarity was verified by checking membrane permeability to fluorescein after incubating the coacervate-supported GUVs with 5 μg/mL melittin. The fluidity of membrane and coacervate phase were characterized through fluorescence recovery after photobleaching (FRAP) experiments. The size of the coacervate-GUVs was modulated by changing the used amount of nanosized liposomes.

Structural and functional stability of coacervate-supported GUVs at extreme environments

The stability of the phospholipid membrane coated coacervates at different NaCl concentration and pH condition were checked by turbidity test. The images of the coacervate-supported GUVs at different extreme environments were taken by the microscope. To evaluate the ability of the membrane coated coacervates to function at extreme environment, HRP was co-assembled with PDDA, ATP, and liposomes, and frozen and thawed to form coacervate-supported GUVs encapsulated with HRP. HRP concentration in the dispersion was 0.5 U/mL. These coacervate-supported GUVs containing HRP were then dispersed in solution media with pH value = 2 and incubated for 60 min. The catalytic ability of HRP in the dispersion was checked by the quantaRed^{TM} enhanced chemifluorescent HRP substrate kit using multi-mode microplate reader. As control, the catalytic ability of HRP (0.5 U/mL) in solution with pH=2 was also checked.

Release of coacervates to form non-supported GUVs

To form non-supported GUVs, we incubated the PDDA-ATP (φ=7/3) coacervate-supported GUVs in solution with 5 μg/mL melittin and 150 mM NaCl. The obtained non-supported GUVs were characterized using the fluorescence microscope to observe their membrane fluctuations and morphology evolution under osmotic shock.